



CHORUS

This is the accepted manuscript made available via CHORUS. The article has been published as:

First-principles calculation of spin-orbit torque in a Co/Pt bilayer

K. D. Belashchenko, Alexey A. Kovalev, and M. van Schilfgaarde

Phys. Rev. Materials **3**, 011401 — Published 29 January 2019

DOI: [10.1103/PhysRevMaterials.3.011401](https://doi.org/10.1103/PhysRevMaterials.3.011401)

First-principles calculation of spin-orbit torque in a Co/Pt bilayer

K. D. Belashchenko,¹ Alexey A. Kovalev,¹ and M. van Schilfhaarde²

¹*Department of Physics and Astronomy and Nebraska Center for Materials and Nanoscience, University of Nebraska-Lincoln, Lincoln, Nebraska 68588, USA*

²*Department of Physics, Kings College London, Strand, London WC2R 2LS, United Kingdom*

(Dated: December 28, 2018)

The angular dependence of spin-orbit torque in a disordered Co/Pt bilayer is calculated using a first-principles non-equilibrium Green's function formalism blue with an explicit supercell averaging over Anderson disorder. In addition to the usual damping-like and field-like terms, the odd torque contains a sizeable planar Hall-like term $(\mathbf{m} \cdot \mathbf{E})\mathbf{m} \times (\mathbf{z} \times \mathbf{m})$ whose contribution to current-induced damping is consistent with experimental observations. The damping-like and planar Hall-like torquances depend weakly on disorder strength, while the field-like torquance declines with increasing disorder. The torques that contribute to damping are almost entirely due to spin-orbit coupling on the Pt atoms, but the field-like torque does not require it.

Spin-orbit torque (SOT)¹, which is a manifestation of relativistic physics in solid-state systems, has attracted considerable interest due to its device applications² in memory technologies³⁻⁷ and spin-torque nano-oscillators⁸⁻¹². SOT can arise in systems lacking bulk inversion symmetry, such as (Ga,Mn)As crystalline systems¹³, or in systems lacking structural inversion symmetry. It can be described in terms of the nonequilibrium spin density¹⁴⁻¹⁶ and can affect the magnetization dynamics¹⁷. For systems containing a heavy metal/ferromagnet interface, two mechanisms of SOT have been suggested: the inverse spin-galvanic effect (ISGE)¹⁸⁻²⁰ arising at a heavy-metal/ferromagnet interface²¹⁻²⁵ and the bulk spin-Hall effect²⁶ originating in the bulk of the heavy metal²⁷⁻²⁹. These mechanisms lead to the field-like $(\mathbf{z} \times \mathbf{E}) \times \mathbf{m}$ and damping-like $\mathbf{m} \times [(\mathbf{z} \times \mathbf{E}) \times \mathbf{m}]$ terms in SOT, which are, respectively, odd and even with respect to the magnetization described by the unit vector \mathbf{m} . Other terms with more complicated angular dependence are allowed by symmetry and have been experimentally identified in several systems³³⁻³⁵. Such contributions can arise due to interfacial scattering alone^{36,37}, without any bulk spin-Hall effect, and are not captured by simple models³⁰⁻³². Axially asymmetric contributions to SOT induced by low crystalline symmetry have also been observed³⁸.

The layers in SOT bilayers are usually made about a nanometer thick or even less. The phenomenological notion of an interface between bulk regions, as well as the interpretation in terms of the bulk spin-Hall effect, is, therefore, unjustified, and a fully quantum-mechanical treatment of the whole device is essential. An extreme case is that of a magnetic layer in contact with a topological insulator (TI)^{39,40}, which can generate strong SOT⁴¹. There is ample experimental evidence of the existence of an interfacial contribution to SOT⁴²⁻⁴⁴. *Ab-initio* studies of Pt/Py bilayers also suggest the importance of interfacial contributions to the spin-Hall effect⁴⁵, which should lead to an interfacial SOT.

Most of the existing *ab-initio* studies of SOT rely on the use of phenomenological broadening for the Green's functions^{16,46}, which does not capture the full physics

of SOT. A calculation of SOT using the coherent potential approximation (CPA) for disorder averaging was also reported⁴⁷, but only one orientation of the magnetization was considered.

In this Letter, we develop the non-equilibrium Green's function (NEGF) approach⁴⁸ within the tight-binding linear muffin-tin orbital (LMTO) method⁴⁹ for *ab-initio* calculations of SOT in magnetic multilayered systems with explicit treatment of disorder and apply it to study SOT in a Co/Pt bilayer. Our results reveal a complicated angular dependence of SOT, including a sizeable planar Hall-like contribution.

In our LMTO-NEGF treatment, spin-orbit coupling is included as a perturbation to the second-order LMTO potential parameters^{50,51}. The spin torque on atom i is calculated as $\mathbf{T}_i = \int \mathbf{B}_{xc,in}(\mathbf{r}) \times \mathbf{m}_{out}(\mathbf{r}) d^3r_i$, where the integral is over the atomic sphere for atom i , $\mathbf{B}_{xc,in}(\mathbf{r})$ is the "input" exchange-correlation field, which is aligned with the prescribed direction of the magnetization, and $\mathbf{m}_{out}(\mathbf{r})$ the "output" magnetization obtained from the NEGF calculation^{16,52-54}. This approach is justified by introducing the constraining fields⁶² stabilizing the instantaneous orientation of magnetization, whereby the internal spin torque is balanced by the torque of the constraining field⁵⁴. The spin-density matrix

$$\hat{\rho}(\mathbf{r}) = -\frac{i}{2\pi} \int_{-\infty}^{\infty} \hat{G}_{<}(E, \mathbf{r}, \mathbf{r}) dE \quad (1)$$

is obtained⁴⁸ from the Green's function $G_{<}$ of the Keldysh formalism, given by

$$G_{<} = iG(f_L\Gamma_L + f_R\Gamma_R)G^\dagger, \quad (2)$$

where G and G^\dagger are the retarded and advanced Green's functions, $\Gamma_{L/R}$ is the anti-Hermitian part of the self-energy for lead L (left) or R (right), and $f_{L/R}(E)$ are the occupation functions for the two leads.

The bias V is applied symmetrically, shifting both the potential and the chemical potential of the left (right) lead by $\pm eV/2$. In the steady state of a homogeneous

metallic conductor with an applied bias, there is a linear potential drop between the leads, while the density is translationally invariant. Thus, instead of performing a self-consistent calculation for the whole system, we impose a linear potential drop and use equilibrium charge and spin densities for all atoms as inputs in the Kohn-Sham Hamiltonian.

Using the identity $G(\Gamma_L + \Gamma_R)G^\dagger = i(G - G^\dagger)$, the integral in Eq. (1) is formally split in two parts referred to as the Fermi-sea and the Fermi-surface contributions:

$$\hat{\rho}_{sea}(\mathbf{r}) = \frac{i}{2\pi} \int \bar{f}(E)(G - G^\dagger)dE \quad (3)$$

$$\hat{\rho}_F(\mathbf{r}) = \frac{eV}{4\pi} \int \left(-\frac{\partial \bar{f}}{\partial E} \right) G(\Gamma_L - \Gamma_R)G^\dagger dE \quad (4)$$

where \bar{f} is the Fermi function with the unperturbed chemical potential, and only the linear term has been kept in (4). This separation is not unique and represents a convenient choice of gauge⁶³. In the Fermi-sea contribution (3), the bias enters through the linear potential drop. The Fermi-sea term can contribute to magnetization damping⁵⁴.

We consider a Co/Pt bilayer with six monolayers each of Co and Pt. The atoms are placed on the sites of the ideal face-centered cubic (fcc) lattice with the lattice pa-

rameter $a = 3.75 \text{ \AA}$, which is approximately half-way between those of fcc Co and Pt. The interface is taken along a (001) plane, and the current direction is [110]. The free surfaces are separated by four monolayers of empty spheres representing vacuum. The length of the active region is 120 monolayers, or 15.9 nm⁵⁴.

The thin-film bilayers used for SOT measurements have rather large resistivities in the 20-100 $\mu\Omega\text{-cm}$ range³³⁻³⁵, reflecting a large degree of disorder. The dominant types of defects responsible for the large residual resistivity are not known. As a generic representation, we use the Anderson disorder model, in which a random potential V_i with a uniform distribution in a range $-V_m < V_i < V_m$ is applied on each site i , including the empty spheres. In order to gain insight about the mechanisms of SOT and its dependence on the relaxation time τ , we considered four values of V_m : 0.77, 1.09, 1.33, and 1.54 eV; the corresponding resistivities range from 23 to 46 $\mu\Omega\text{-cm}$ ⁵⁴.

The total torque \mathbf{T} is split into two parts: $\mathbf{T} = \mathbf{T}_e + \mathbf{T}_o$, which are, respectively, even and odd with respect to \mathbf{m} . The crystallographic symmetry of the bilayer is C_{4v} . We align the x axis with the current direction [110] and z with [001], which is normal to the film plane. Group-theoretical analysis gives the allowed terms in the angular dependence of SOT:

$$\begin{aligned} \mathbf{T}_e = & P(\{A\}, \theta) \mathbf{m} \times [(\mathbf{z} \times \mathbf{E}) \times \mathbf{m}] + P(\{A'\}, \theta) (\mathbf{m} \cdot \mathbf{E}) \mathbf{z} \times \mathbf{m} \\ & + P(\{A_\alpha\}, \theta) m_z (m_x^2 - m_y^2) \mathbf{m} \times (E_x, -E_y, 0) + P(\{A_\beta\}, \theta) [(m_x^2 - m_y^2) (\mathbf{m} \times \mathbf{z})(E_x m_x - E_y m_y) - \langle \dots \rangle] + \dots \end{aligned} \quad (5)$$

$$\mathbf{T}_o = P(\{B\}, \theta) (\mathbf{z} \times \mathbf{E}) \times \mathbf{m} + P(\{B'\}, \theta) (\mathbf{m} \cdot \mathbf{E}) \mathbf{m} \times (\mathbf{z} \times \mathbf{m}) + P(\{B_\alpha\}, \theta) (m_x^2 - m_y^2) \mathbf{m} \times (E_y, E_x, 0) + \dots \quad (6)$$

Here $\{X\}$ denotes a set of coefficients X_{2n} , $n = 0, 1, \dots$, and $P(\{X\}, \theta) = \sum_n X_{2n} P_{2n}(\cos \theta)$ is a linear combination of even Legendre polynomials. The A , A' , B , B' terms are allowed in a system with axial symmetry group $C_{\infty v}$, while the A_α , A_β , B_α terms appear once the symmetry is reduced to C_{4v} . A_0 and B_0 represent the conventional damping-like and field-like SOT terms, respectively.

The brackets $\langle \dots \rangle$ in Eq. (5) stand for the average of the preceding term over the axial rotations of the bilayer (which is proportional to the corresponding A'_0 term). Such averages already vanish for the A_α and B_α terms. In the axially symmetric polycrystalline sample with (001) texture, the predicted angular dependence is given by the A , A' , B , and B' terms only.

In all calculations we have $\mathbf{E} = E\hat{x}$, and the torquances are defined as $\boldsymbol{\tau}_e = \mathbf{T}_e/(ME)$, $\boldsymbol{\tau}_o = \mathbf{T}_o/(ME)$, where M is the total magnetization, and have the dimension of a magnetoelectric coefficient $[B/E] = \text{ns/m} = \text{T} \cdot \text{nm/V}$.

The contribution of SOT to magnetization damping

α , which is obtained in ferromagnetic resonance (FMR) linewidth measurements³⁵, is $\Delta\alpha = C(E/B)$, where

$$C = \mathbf{m} \cdot \nabla_{\mathbf{m}} \times [\mathbf{m} \times \boldsymbol{\tau}(\mathbf{m})] \quad (7)$$

is the negative curl of the effective field⁵⁴.

The Fermi-sea term is calculated in the middle of the device with a finite bias of order 1 mV applied symmetrically, as required by Eq. (3)-(4), without disorder. Equilibrium torque from the magnetic anisotropy is removed by subtracting the torque at positive and negative bias. To avoid the formidable task of evaluating the integral in Eq. (3), the Fermi-sea term is calculated at a finite temperature, using the integration method of Ref. 64. The integrand only needs to be calculated at a finite number of points on the imaginary axis, most of which allow a coarse mesh in the reciprocal-space integral. The Fermi-sea term, which is strictly even, is calculated for 61 orientations of the magnetization⁶⁵ and then fitted to Eq. (5). We have verified that the Fermi-sea torque depends

linearly on the bias voltage, is insensitive to the length of the active region at constant field, and vanishes if the linear potential drop is replaced by two abrupt steps at the edges of the active region.

The Fermi-sea torques obtained for $T = 50, 100, 200,$ and 300 K are shown in Fig. 1. The minimal set of terms giving an acceptable fit at all temperatures includes $A_0, A_2, A'_0,$ and $A_{\beta 0}$ (see Table I); a more accurate multi-parametric fit is used to compute the parameter C shown in Fig. 1. A'_0 is the largest term in the minimal fit, and it becomes quite large at low temperatures. A_2 and $A_{\beta 0}$ are also important at lower T , although $A_{\beta 0}$ should average out in polycrystalline samples.

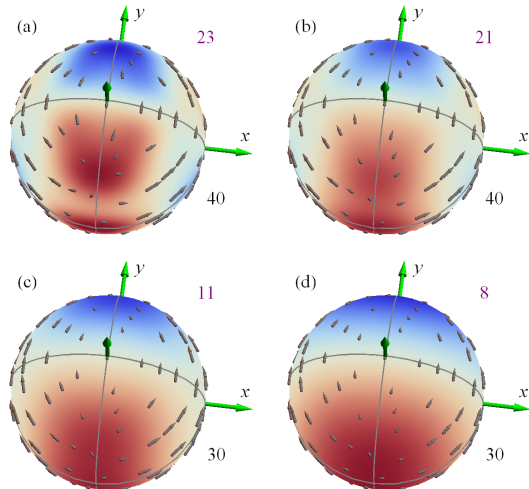


FIG. 1. Fermi sea contribution to the torque τ_e (arrows) at (a) 50 K, (b) 100 K, (c) 200 K, (d) 300 K. The intensity of red (blue) color shows the positive (negative) magnitude of the damping parameter C [Eq. (7)]. In each panel, the number on bottom right gives the scale of an arrow with a length equal to the sphere radius, and one on top right gives the color map scale (both in ns/m).

The integrand in Eq. (4) for the Fermi-surface term contains a delta-function at zero temperature and needs to be calculated only near the Fermi level E_F . The temperature dependence of this term is determined primarily by τ rather than the temperature in the Fermi distribution function. The reciprocal-space integration requires about 1000 points to keep the relative errors within a few percent. The Fermi surface contribution to the total torque, summed up over all sites in the active region, is calculated for 32 orientations of the magnetization, which form 16 antiparallel pairs, and averaged over a sufficient number of disorder configurations⁶⁶. The symmetric and antisymmetric parts of the torque are then fitted to Eqs. (5) and (6). Only $A_0, A'_0, B_0,$ and B'_0 coefficients turned out to be sizeable; they are listed in Table I. With the exception of A'_0 , all coefficients depend weakly on the transverse supercell size L_y , confirming the reliability of disorder averaging. The fitted expressions were used to evaluate the damping parameter C , and the

results are displayed in Fig. 2 for two strengths of disorder, $V_m = 0.77$ and 1.54 eV.

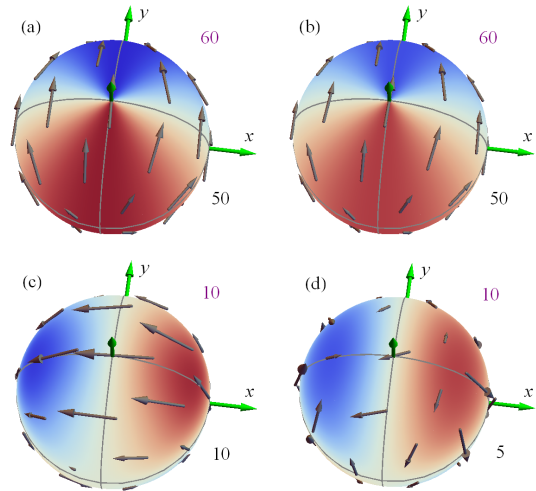


FIG. 2. Fermi surface contribution to the torque (arrows): (a) τ_e at $V_m = 0.77$ eV, (b) τ_e at $V_m = 1.54$ eV, (c) τ_o at $V_m = 0.77$ eV, (d) τ_o at $V_m = 1.54$ eV. The scales are indicated as in Fig. 1. Supercells with $L_y = 2$ were used for disorder averaging.

The Fermi-surface contribution to the even torque is dominated by the simple damping-like term A_0 . The leading contribution to damping from the even torque is given by $C = -(2A_0 + A'_0)m_y$. Although the Fermi-surface part of A'_0 converges slowly with the transverse supercell size L_y , it is clear from Table I that its contribution to C is small compared to A_0 .

Table I shows that, as the disorder strength increases from 0.77 to 1.54 eV, the A_0 term remains essentially constant, while the resistivity and the resistance of the active region increase by more than a factor of 2^{54} . This shows that the damping-like torque A_0 depends weakly on τ . The magnitude of A_0 is consistent with experimental data⁶⁷ for a Co/Pt bilayer with similar layer thicknesses, as well as with prior calculations using phenomenological broadening⁴⁶. These observations suggest that damping-like SOT in this bilayer is dominated by intrinsic band-structure effects.

In addition to the simple field-like B_0 term, the odd torque contains a sizeable B'_0 term of comparable magnitude (see Table I); other terms are relatively small. This is in contrast to calculations based on phenomenological broadening⁴⁶, where no terms beyond B_0 were found. The B_0 coefficient decreases with increasing disorder strength, as expected for ISGE. However, the relatively large error bar for B_0 , which is evident from its dependence on L_y , does not allow us to predict its temperature dependence at constant current density.

The mechanisms of SOT are closely related to its temperature dependence through their dependence on τ . The intrinsic damping-like SOT is independent of τ at a fixed electric field, and hence it should be proportional

TABLE I. Coefficients (ns/m) in the angular expansion of the spin-orbit torque in the Co/Pt bilayer. L_y is the lateral supercell size in the units of $a/\sqrt{2}$ (only relevant for the Fermi-surface part). E is the energy; $E_{\pm} = E_F \pm 0.046$ eV.

	E	L_y	Fermi surface, V_m (eV)				Fermi sea, T (K)			
			0.77	1.09	1.33	1.54	300	200	100	50
A_0	E_F	1	29.4	24.8	23.4	21.9	1.4	0.8	0.8	-1.3
	E_F	2	29.9	31.3	24.4	27.7				
	E_F	3		27.5						
	E_+	2		30.5						
	E_-	2		26.8						
A'_0	E_F	1	-5.2	-3.1	-2.6	-0.7	5.3	7.6	10.6	13.6
	E_F	2	-3.3	-10.7	-2.8	-7.5				
	E_F	3		-6.0						
	E_+	2		-4.7						
	E_-	2		-2.2						
A_2	E_F	2	-1.3	-2.2	-0.3	-0.9	0.6	1.4	3.2	6.3
$A_{\beta 0}$	E_F	2	-1.5	-0.3	0.0	0.0	0.3	1.4	5.2	7.3
B_0	E_F	1	-8.1	-8.0	-6.3	-4.1				0
	E_F	2	-8.8	-5.0	-3.8	-1.7				
	E_F	3		-6.3						
	E_+	2		-7.5						
	E_-	2		-3.2						
B'_0	E_F	1	-6.8	-8.2	-10.7	-9.9				0
	E_F	2	-7.5	-7.6	-6.8	-5.8				
	E_F	3		-8.3						
	E_+	2		-9.3						
	E_-	2		-8.3						

to the resistivity $\rho(T)$ at a constant current density. Although the field-like SOT due to interfacial ISGE scales with τ similar to the conductivity, the interfacial and bulk scattering rates may be different.

There are few experimental measurements of the temperature dependence of SOT, and they are poorly understood. In Ta-based systems the field-like SOT was reported to increase quickly with temperature while the resistivity and the damping-like SOT are nearly constant^{68,69}. This behavior is inconsistent with the ISGE mechanism of the field-like-SOT. Temperature dependence of the field-like SOT is different in as-grown Pt/Co and annealed Pt/CoFeB bilayers⁷⁰. The unexpected temperature dependence of the field-like SOT suggests that processes involving phonons or magnons may play an important role^{1,71}.

The terms B'_0 and B_2 in the odd torque contribute to damping as $C = 3(B'_0 + B_2)m_x m_z$, which is the “planar Hall-like” damping observed when \mathbf{m} lies in the xz plane³⁵. Table I shows that the term B'_0 is not sensitive to disorder strength, similarly to A_0 . The B_2 term was found to be small in all cases.

The existence of large terms beyond B_0 in the odd SOT is consistent with experimental observations³³⁻³⁵. However, while we found large B'_0 and $B_2 \approx 0$ in a Co/Pt

bilayer, measurements of SOT in $\text{AlO}_x/\text{Co}/\text{Pt}$ ³³ and $\text{AlO}_x/\text{Co}/\text{Pd}$ ³⁴ suggest an approximate relation $B_2 = -\frac{2}{3}B'_0$ in these systems⁵⁴. The relative magnitude of the damping parameter C measured in the xy (spin-Hall-like SOT) and xz planes (planar Hall-like SOT) agrees with FMR linewidth measurements³⁵, but the sign of B'_0 is different. This disagreement may be due the inadequacy of the Anderson disorder model. Indeed, weak dependence of B'_0 on disorder strength (see Table I) and the absence of any terms beyond B_0 in calculations based on band broadening⁴⁶ suggest that these terms arise from vertex corrections, which are sensitive to the type of disorder present in the system.

Table I also lists the Fermi-surface SOT coefficients calculated at energies $E_{\pm} = E \pm 0.046$ eV, where $(-\partial f/\partial E)$ is reduced by 50% compared to its maximal value at 300 K. Weak energy dependence of A_0 and B'_0 , and approximately linear dependence of B_0 , suggests that these coefficients are not sensitive to the Fermi temperature. The A'_0 coefficient remains small.

For further insight in the origin of SOT, Fig. 3 shows atom-resolved contributions to the A_0 , A'_0 , B_0 , and B'_0 terms at $V_m = 1.09$ eV. For comparison, these quantities are also shown for the free-standing 6-monolayer Co film with the same lattice parameter, where the total torque vanishes by symmetry.

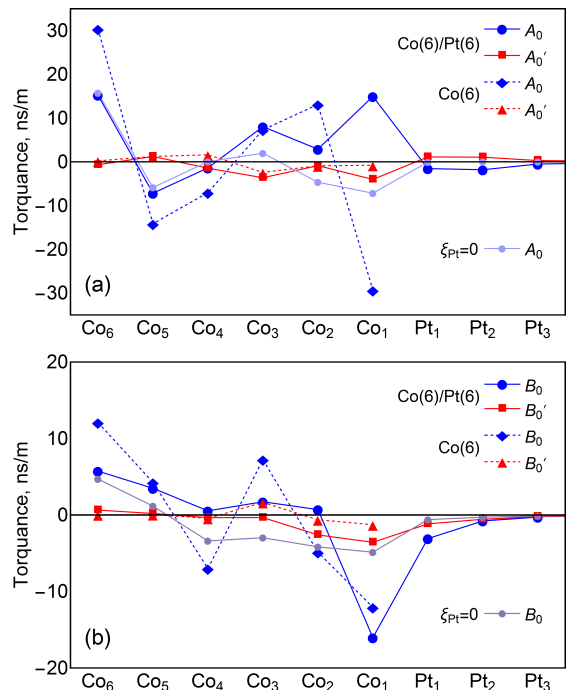


FIG. 3. Atom-resolved torquances in the Co(6)Pt(6) bilayer (solid lines) and in the free-standing Co(6) film (dashed lines) at $V_m = 1.09$ eV, obtained with $L_y = 3$. (a) Even terms A_0 and A'_0 , (b) odd terms B_0 and B'_0 . Light-blue curves (labeled $\xi_{Pt} = 0$): A_0 in Co(6)Pt(6) with SOC on Pt atoms set to zero, obtained with $L_y = 1$.

The contributions to A_0 and B_0 are spread throughout

the thickness of the film, with the largest contributions coming from the Co atoms at the Co/Pt interface and at the free surface of Co. On the other hand, the B'_0 term appears to originate at the Co/Pt interface. It is interesting to observe a considerable contribution to B_0 from the Pt atoms near the interface, which carry a magnetic moment of about $0.24\mu_B$ thanks to the magnetic proximity effect⁷². In fact, SOT on the Pt atoms contributes as much as 40% of the total magnitude of B_0 . Surprisingly, the atom-resolved contributions at the surface Co atoms in the free-standing Co film are even larger in magnitude than those at the Co/Pt interface.

Finally, we examine the SOT with the SOC on Pt atoms switched off, using the supercell with $L_y = 2$. The A_0 term essentially disappears, but, as seen in Fig. 3(a), atom-resolved contributions remain sizeable, and those near the free Co surface barely change. The B'_0 term is strongly suppressed from -7.6 to -1.4 ns/m, which is comparable to the averaging error. On the other hand, the B_0 term increases to -10.8 ns/m, with strongly redistributed atom-resolved contributions [Fig. 3(b)]. These results suggest that, without SOC on Pt, the SOT in our Co/Pt bilayer is nearly non-dissipative, i.e., it does not affect magnetization damping. Current-induced Dzyaloshinskii-Moriya interaction⁷³ formally leads to damping-like atom-resolved torques that add up to zero⁵⁴. Thus, strong field-like SOT does not require a heavy-metal layer, but understanding the prerequisites

for observing damping-like SOT without heavy metals⁷⁴ will require further research.

In conclusion, we have demonstrated the feasibility of calculating the SOT for a Co/Pt bilayer with an explicit model of disorder within the NEGF formalism based on density-functional theory. Terms beyond the usual damping-like and field-like torques were found, including a sizeable planar Hall-like B'_0 term [Eq. (6)], consistent with FMR measurements³⁵. The dissipative part of SOT is almost entirely due to SOC on Pt atoms.

ACKNOWLEDGMENTS

We thank Vladimir Antropov, Gerrit Bauer, Ilya Krivorotov, Farzad Mahfouzi, Branislav Nikolić, Yaroslav Tserkovnyak, and Igor Žutić for useful discussions. The work at UNL was supported by the National Science Foundation (NSF) through Grant No. DMR-1609776 and the Nebraska Materials Research Science and Engineering Center (MRSEC, Grant No. DMR-DMR-1420645). A.K. was supported by the U.S. Department of Energy, Office of Science, Basic Energy Sciences, under Award No. DE-SC0014189. M.v.S. was supported by the EP-SRC CCP9 Flagship Project No. EP/M011631/1. Calculations were performed utilizing the Holland Computing Center of the University of Nebraska, which receives support from the Nebraska Research Initiative.

-
- ¹ A. Manchon, I. M. Miron, T. Jungwirth, J. Sinova, J. Zelezny, A. Thiaville, K. Garello, and P. Gambardella, ArXiv e-prints (2018), arXiv:1801.09636.
- ² R. Ramaswamy, J. M. Lee, K. Cai, and H. Yang, Appl. Phys. Rev. **5**, 031107 (2018).
- ³ K. Garello, C. O. Avci, I. M. Miron, M. Baumgartner, A. Ghosh, S. Auffret, O. Boulle, G. Gaudin, and P. Gambardella, Appl. Phys. Lett. **105**, 212402 (2014).
- ⁴ S.-H. Yang, K.-S. Ryu, and S. Parkin, Nat. Nanotechnol. **10**, 221 (2015).
- ⁵ S. V. Aradhya, G. E. Rowlands, J. Oh, D. C. Ralph, and R. A. Buhrman, Nano Lett. **16**, 5987 (2016).
- ⁶ G. Prenat, K. Jabeur, P. Vanhauwaert, G. D. Pendina, F. Oboril, R. Bishnoi, M. Ebrahimi, N. Lamard, O. Boulle, K. Garello, J. Langer, B. Ocker, M. Cyrille, P. Gambardella, M. Tahoori, and G. Gaudin, IEEE Trans. Multi-Scale Computing Syst. **2**, 49 (2016).
- ⁷ S. Fukami and H. Ohno, Jpn. J. Appl. Phys. **56**, 0802A1 (2017).
- ⁸ L. Liu, C.-F. Pai, D. C. Ralph, and R. A. Buhrman, Phys. Rev. Lett. **109**, 186602 (2012).
- ⁹ V. E. Demidov, S. Urazhdin, H. Ulrichs, V. Tiberkevich, A. Slavin, D. Baither, G. Schmitz, and S. O. Demokritov, Nat. Mater. **11**, 1028 (2012).
- ¹⁰ Z. Duan, A. Smith, L. Yang, B. Youngblood, J. Lindner, V. E. Demidov, S. O. Demokritov, and I. N. Krivorotov, Nat. Commun. **5**, 5616 (2014).
- ¹¹ M. Collet, X. de Milly, O. D'Allivy Kelly, V. V. Naletov, R. Bernard, P. Bortolotti, J. Ben Youssef, V. E. Demidov, S. O. Demokritov, J. L. Prieto, M. Muñoz, V. Cros, A. Anane, G. de Loubens, and O. Klein, Nat. Commun. **7**, 10377 (2016).
- ¹² A. A. Awad, P. Dürrenfeld, A. Houshang, M. Dvornik, E. Iacocca, R. K. Dumas, and J. Åkerman, Nat. Phys. **13**, 292 (2017).
- ¹³ H. Kurebayashi, J. Sinova, D. Fang, A. C. Irvine, T. D. Skinner, J. Wunderlich, V. Novák, R. P. Campion, B. L. Gallagher, E. K. Vehstedt, L. P. Zárbo, K. Výborný, A. J. Ferguson, and T. Jungwirth, Nat. Nanotechnol. **9**, 211 (2014).
- ¹⁴ I. Garate and A. H. MacDonald, Phys. Rev. B **80**, 134403 (2009).
- ¹⁵ A. Manchon and S. Zhang, Phys. Rev. B **79**, 094422 (2009).
- ¹⁶ F. Freimuth, S. Blügel, and Y. Mokrousov, Phys. Rev. B **90**, 174423 (2014).
- ¹⁷ K. Ando, S. Takahashi, K. Harii, K. Sasage, J. Ieda, S. Maekawa, and E. Saitoh, Phys. Rev. Lett. **101**, 036601 (2008).
- ¹⁸ A. Aronov and Y. B. Lyanda-Geller, JETP Lett. **50**, 431 (1989).
- ¹⁹ V. M. Edelstein, Solid State Commun. **73**, 233 (1990).
- ²⁰ S. D. Ganichev, M. Trushin, and J. Schliemann, in Handbook of spin transport and magnetism, ed. E. Y. Tsymbal and I. Žutić (CRC, Boca Raton, FL, 2011), p. 487.
- ²¹ A. Chernyshov, M. Overby, X. Liu, J. K. Furdyna, Y. Lyanda-Geller, and L. P. Rokhinson, Nat. Phys. **5**, 656 (2009).
- ²² I. M. Miron, G. Gaudin, S. Auffret, B. Rodmacq,

- A. Schuhl, S. Pizzini, J. Vogel, and P. Gambardella, *Nat. Mater.* **9**, 230 (2010).
- ²³ I. M. Miron, K. Garello, G. Gaudin, P.-J. Zermatten, M. V. Costache, S. Auffret, S. Bandiera, B. Rodmacq, A. Schuhl, and P. Gambardella, *Nature* **476**, 189 (2011).
- ²⁴ A. Manchon, H. C. Koo, J. Nitta, S. M. Frolov, and R. A. Duine, *Nat. Mater.* **14**, 871 (2015).
- ²⁵ X. Fan, H. Celik, J. Wu, C. Ni, K.-J. Lee, V. O. Lorenz, and J. Q. Xiao, *Nat. Commun.* **5**, 3042 (2014).
- ²⁶ J. Sinova, S. O. Valenzuela, J. Wunderlich, C. H. Back, and T. Jungwirth, *Rev. Mod. Phys.* **87**, 1213 (2015).
- ²⁷ L. Liu, T. Moriyama, D. C. Ralph, and R. A. Buhrman, *Phys. Rev. Lett.* **106**, 036601 (2011).
- ²⁸ L. Liu, C.-F. Pai, Y. Li, H. W. Tseng, D. C. Ralph, and R. A. Buhrman, *Science* **336**, 555 (2012).
- ²⁹ L. Liu, O. J. Lee, T. J. Gudmundsen, D. C. Ralph, and R. A. Buhrman, *Phys. Rev. Lett.* **109**, 096602 (2012).
- ³⁰ A. Qaiumzadeh, R. Å. A. Duine, and M. Titov, *Phys. Rev. B* **92**, 014402 (2015).
- ³¹ I. A. Ado, O. A. Tretiakov, and M. Titov, *Phys. Rev. B* **95**, 094401 (2017).
- ³² C. Xiao and Q. Niu, *Phys. Rev. B* **96**, 045428 (2017).
- ³³ K. Garello, I. M. Miron, C. O. Avci, F. Freimuth, Y. Mokrousov, S. Blügel, S. Auffret, O. Boule, G. Gaudin, and P. Gambardella, *Nat. Nanotechnol.* **8**, 587 (2013).
- ³⁴ A. Ghosh, K. Garello, C. O. Avci, M. Gabureac, and P. Gambardella, *Phys. Rev. Applied* **7**, 014004 (2017).
- ³⁵ C. Safranski, E. A. Montoya, and I. N. Krivorotov, *Nat. Nanotechnol.*, <https://doi.org/10.1038/s41565-018-0282-0> (2018).
- ³⁶ V. P. Amin and M. D. Stiles, *Phys. Rev. B* **94**, 104419 (2016).
- ³⁷ V. P. Amin and M. D. Stiles, *Phys. Rev. B* **94**, 104420 (2016).
- ³⁸ D. MacNeill, G. M. Stiehl, M. H. D. Guimaraes, R. A. Buhrman, J. Park, and D. C. Ralph, *Nat. Phys.* **13**, 300 (2017).
- ³⁹ F. Mahfouzi, B. K. Nikolić, and N. Kioussis, *Phys. Rev. B* **93**, 115419 (2016).
- ⁴⁰ J.-P. Hanke, F. Freimuth, C. Niu, S. Blügel, and Y. Mokrousov, *Nat. Commun.* **8**, 1479 (2017).
- ⁴¹ A. R. Mellnik, J. S. Lee, A. Richardella, J. L. Grab, P. J. Mintun, M. H. Fischer, A. Vaezi, A. Manchon, E.-A. Kim, N. Samarth, and D. C. Ralph, *Nature* **511**, 449 (2014).
- ⁴² J. Kim, J. Sinha, M. Hayashi, M. Yamanouchi, S. Fukami, T. Suzuki, S. Mitani, and H. Ohno, *Nat. Mater.* **12**, 240 (2013).
- ⁴³ R. Ramaswamy, X. Qiu, T. Dutta, S. D. Pollard, and H. Yang, *Appl. Phys. Lett.* **108**, 202406 (2016).
- ⁴⁴ J. Torrejon, J. Kim, J. Sinha, S. Mitani, M. Hayashi, M. Yamanouchi, and H. Ohno, *Nat. Commun.* **5**, 4655 (2014).
- ⁴⁵ L. Wang, R. J. H. Wesselink, Y. Liu, Zh. Yuan, K. Xia, and P. J. Kelly, *Phys. Rev. Lett.* **116**, 196602 (2016).
- ⁴⁶ F. Mahfouzi and N. Kioussis, *Phys. Rev. B* **97**, 224426 (2018).
- ⁴⁷ S. Wimmer, K. Chadova, M. Seemann, D. Ködderitzsch, and H. Ebert, *Phys. Rev. B* **94**, 054415 (2016).
- ⁴⁸ S. V. Faleev, F. Léonard, D. A. Stewart, and M. van Schilfgaarde, *Phys. Rev. B* **71**, 195422 (2005).
- ⁴⁹ I. Turek, V. Drchal, J. Kudrnovský, M. Šob, and P. Weinberger, *Electronic Structure of Disordered Alloys, Surfaces and Interfaces* (Kluwer, Boston, 1997).
- ⁵⁰ I. Turek, V. Drchal, and J. Kudrnovský, *Philos. Mag.* **88**, 2787 (2008).
- ⁵¹ K. D. Belashchenko, L. Ke, M. Däne, L. X. Benedict, T. N. Lamichhane, V. Taufour, A. Jesche, S. L. Bud'ko, P. C. Canfield, and V. P. Antropov, *Appl. Phys. Lett.* **106**, 062408 (2015).
- ⁵² P. M. Haney, D. Waldron, R. A. Duine, A. S. Nunez, H. Guo, and A. H. MacDonald, *Phys. Rev. B* **76**, 024404 (2007).
- ⁵³ B. K. Nikolić, K. Dolui, M. D. Petrović, P. Plecháč, T. Markussen, and K. Stokbro, in *Handbook of Materials Modeling: Applications: Current and Emerging Materials* (Springer, Cham, 2018), p. 1.
- ⁵⁴ The formula for the spin torque, the origin of the Fermi-sea contribution to the damping-like torque, aspects of angular dependence, the band structure, and calculations of the resistivities are discussed in the Supplementary Material, which includes Refs. 55–61.
- ⁵⁵ S. A. Turzhevskii, A. I. Lichtenstein, and M. I. Katsnelson, *Sov. Phys.–Solid State* **32**, 1138 (1990).
- ⁵⁶ V. P. Antropov and A. I. Lichtenstein, *MRS Symp. Proc.* **253**, 325 (1992).
- ⁵⁷ V. P. Antropov, M. I. Katsnelson, B. N. Harmon, M. van Schilfgaarde, and D. Kusnezov, *Phys. Rev. B* **54**, 1019 (1996).
- ⁵⁸ S. V. Halilov, H. Eschrig, A. Y. Perlov, and P. M. Oppeneer, *Phys. Rev. B* **58**, 293 (1998).
- ⁵⁹ E. Runge and E. K. U. Gross, *Phys. Rev. Lett.* **52**, 997 (1984).
- ⁶⁰ K. Capelle, G. Vignale, and B. L. Györfy, *Phys. Rev. Lett.* **87**, 206403 (2001).
- ⁶¹ G. M. Stocks, B. Ujfalussy, X. Wang, D. M. C. Nicholson, W. A. Shelton, Y. Wang, A. Canning, and B. L. Györfy, *Philos. Mag. B* **78**, 665 (1998).
- ⁶² P. H. Dederichs, S. Blügel, R. Zeller, and H. Akai, *Phys. Rev. Lett.* **53**, 2512 (1984).
- ⁶³ F. Mahfouzi and B. K. Nikolić, *SPIN* **03**, 1330002 (2013).
- ⁶⁴ T. Ozaki, *Phys. Rev. B* **75**, 035123 (2007).
- ⁶⁵ The 61 pairs of points on the sphere include 12 vertices, 20 face centers, and 30 edge centers of an icosahedron, plus 60 vertices of a buckyball.
- ⁶⁶ Because the terms in Eq. (4) with Γ_L and Γ_R give identical contributions to the odd torque, it is advantageous to average these terms independently over different disorder configurations.
- ⁶⁷ M.-H. Nguyen, D. C. Ralph, and R. A. Buhrman, *Phys. Rev. Lett.* **116**, 126601 (2016).
- ⁶⁸ J. Kim, J. Sinha, S. Mitani, M. Hayashi, S. Takahashi, S. Maekawa, M. Yamanouchi, and H. Ohno, *Phys. Rev. B* **89**, 174424 (2014).
- ⁶⁹ X. Qiu, P. Deorani, K. Narayanapillai, K.-S. Lee, K.-J. Lee, H.-W. Lee, and H. Yang, *Sci. Rep.* **4**, 4491 (2014).
- ⁷⁰ C. F. Pai, Y. Ou, L. H. Vilela-Leao, D. C. Ralph, and R. A. Buhrman, *Phys. Rev. B* **92**, 064426 (2015).
- ⁷¹ Y. Cheng, K. Chen, and S. Zhang, *Phys. Rev. B* **96**, 024449 (2017).
- ⁷² I. Žutić, A. Matos-Abiague, B. Scharf, H. Dery, and K. Belashchenko, *Mater. Today*, in press, <https://doi.org/10.1016/j.mattod.2018.05.003> (2018).
- ⁷³ F. Freimuth, S. Blügel, and Y. Mokrousov, arXiv:1806.04782.
- ⁷⁴ M. Haidar, A. A. Awad, M. Dvornik, R. Khymyn, A. Houshang, and J. Åkerman, arXiv:1808.09330.